American Journal of Aerospace Engineering
2026, Vol. 12, No. 1, pp. 12–27
https://doi.org/10.11648/j.ajae.20261201.12

Methodology Article

Development of Algorithms and Computer Codes for the Aerodynamic Configurational Design

Satish Chander Gupta*

Department of Aeronautical and Aerospace Engineering, Manikudi Venkataraman Jayaraman College of Engineering, Bangalore, India

Abstract

Several algorithms and computer codes are developed for the configurational aerodynamic design. Mathematical background, physics involved and their applications are brought out. These range from subsonic to supersonic, including transonic Mach number. Vortex lattice method is applied for handling subsonic and supersonic flow conditions under the linearised flow regime. Finite difference methodology is applied for transonic flow nonlinearities. Matrix of optimization is formed through principles of calculus of variations. The codes developed provide capabilities for inverse design for given loading, aerodynamic drag reduction, high lift to drag designs, generation of morphed profiles, wing optimization in the presence of canard, control surfaces sizing, design of reflex camber wings, and effect of ground proximity on flare manoeuvre, Analysis and Design is made over larger domain of flow field. Details on Camber morphing of wings are elaborated. Camber-morphing aerofoils aim to achieve their camber changes in a smooth way to potentially reduce the drag penalty. Morphing is possible by applying optimisation while restraining variation in camber in certain portions of the wing. A matrix for morphing is developed and scheme so developed is applied herein. Morphing as a concept is also applied to optimise wing for minimum induced drag in the presence of canard, where the slopes of canard camber are made to remain invariant to changes. As the aircraft comes close to ground during landing, runway interferes with aircraft flow field. Some aspects of interference effects of solid boundary wall are established. The influence of wall boundaries on the wing is estimated. Wing is placed at different heights above a horizontal solid surface plane, and an equal opposite vortex system is placed at depth equal to height below this surface. Codes developed find a useful application for design of aircraft for several aspects.

Keywords

Optimisation, Morphing, Canard Coupling, Transonic Flow, Ground Interference

1. Introduction

Capabilities of codes include generation of optimal camber shapes for max range and endurance conditions, morphing of wings, canard-wing interactions, transonic and supersonic flow field analysis, inverse designs, estimation of differential loads, effect of runway presence for modelling of flare manoeuvres. Vortex lattice method is applied for handling subsonic and supersonic flow conditions under the linearised flow regime. Finite difference methodology is applied for transonic flow nonlinearities. Reduction in induced drag is considered

*Correspondence: Satish Chander Gupta (satish_chander_gupta@yahoo.co.in)

Received: 5 May 2026; **Accepted:** 16 May 2026; **Published:** 12 June 2026

as the objective for the shape optimization. Matrix of optimization is formed through principles of calculus of variations. In the supersonic regime influence towards downwash is considered from an upstream Mach cone. Objective function for drag minimum is subjected to constrained value of lift or a combination of lift and pitching moment constraint. Value of lift can be incremented, and the value of pitching moment can be decremented while solving for the matrix of optimisation. Later of which produces reflex camber. Such a design has practical application for tailless aircraft. Initially a flat surface is considered for optimization. The resulting optimal warp is split into twist and camber. Angle-of-attack is alleviated by the value of washout at root, and camber is also reduced by this value. Thus, maintaining the same value of lift coefficient and aerodynamic efficiency at a reduced angle-of-attack for the optimized wing. Maximum range or maximum endurance criteria is applied to generate camber to meet the required induced drag values. Codes developed include the capability to handle differential loading i.e. aileron deployment and/or rolling motion including aeroelastic effects.

Camber-morphing aerofoils aim to achieve their camber change in a smooth way to potentially reduce the drag penalty. Morphing technology involves in altering the aircraft's shape, structure, or surface characteristics in real-time in response to external conditions. By adapting the shape and structural features of wings, morphing aircraft can achieve improved lift-to-drag ratios, superior flight performance, and increased versatility across various mission profiles. Morphing is possible by applying optimisation while restraining variation in camber in certain portion of the wing. A matrix for morphing is developed and scheme so developed is applied herein. Morphing as a concept is also applied to optimise wing for minimum induced drag in the presence of canard, where the slopes of canard camber are made to remain invariant to changes.

Computations of transonic flow is progressed on the developed aerofoils to check for presence of shock waves in a bid to establish critical Mach number where the drag rise is high. Algorithm and physics for application of transonic flow equations is developed. Computations of transonic flow are progressed for two different wing configurations.

As the aircraft comes close to ground during landing, a flare manoeuvre is executed. Some aspects of time constant and interference effects of solid boundary wall are established. The influence of wall boundaries on the wing is estimated. Wing is placed at different heights `h` represented by `h/b` above a horizontal solid surface plane, and an equal opposite vortex system is placed at depth `h` below this surface. The vertical velocity component induced at any point on the solid surface plane by the wing is equal and opposite to that due to the inverted mirror image of wing at distance `h` below the ground surface. This satisfies the solid surface requirement that there should not be component of vertical velocity across a solid surface. The heigh `h` is varied to study its influence on the aerodynamic coefficients. Inverted image of given wing is referred to as `carbon wing`.

The computer programs are developed in FORTRAN language, and Gfortran complier of Fedora-12 Operating System (OS) is used to run these programs. Fedora-12 is supported on LINUX platform of VMware and is an open licence that is available for free-download. The programs are run on a 64-bit double precision Laptop.

Following commands comply and create a binary ready for executions.

gfortran -o program name program name.f

Following command executes the

./program name<input file name

Computer codes so developed are useful for educational purposes, research and innovative projects and can be applied for design studies of aircraft.

2. Mathematical Formulation

Subsonic and Supersonic flows: Ideal flow without the effect of viscosity is modelled here since such flows can be regarded as potential flows that are useful for configurational aerodynamic purposes in linearity and steady conditions. In the approach made here, wings are represented by a large number of vortex Lattice panels to model circulation. These panels are used for estimation of pressure difference coefficients. Circulation is determined through tangential flow boundary conditions. Programs developed generate the output matrix of pressure difference coefficients from where lift, induced drag and moments are determined. Thereafter optimization constraint of the lift is introduced i.e., lift before and after the optimization is maintained as same. It can also be increased by multiplying with a factor referred to as `LIF`. Due to the effort of optimization, the wing becomes cambered and gets twisted thereby creating washout [1-5]. Figure 1 shows the axis system, paneling scheme and related moments. Objective function (F) for the drag minima and specified value of lift ($\bar{L}$) are written in Lagrange form using Lagrange multiplier λ_0 as below:

$$F = D + \lambda_0(LIF \times L - \bar{L}) \tag{1}$$

Lift is obtained from the following expression:

$$L = \rho U[A_1\gamma_1 + \cdots + A_N\gamma_N] \tag{2}$$

Here, γ_1, γ_N are circulation strength of N number of panels & A_1,..A_N are related panel areas. Lift can be incremented either by raising alpha or through a multiplication factor. Matrix of optimization is given by Eq. (3) that is obtained by differentiating objective function (F) w.r.t circulation.

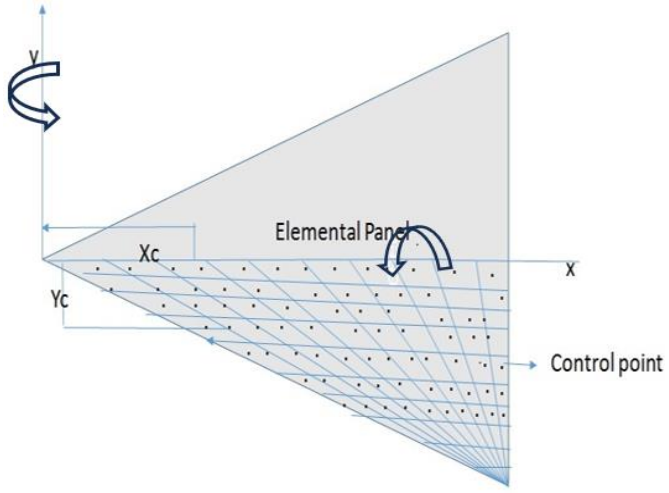

Figure 1. *Axis system, paneling scheme and moments.*

$$\begin{bmatrix} 2A_1a_{1,1} & . & . & . & (A_1a_{1,N}+A_Na_{N,1}) & A_1 \\ . & & & & . & . \\ . & & & & . & . \\ . & & & & . & . \\ (A_Na_{N,1}+A_1a_{1,N}) & . & . & . & 2A_Na_{N,N} & A_N \\ A_1 & . & . & . & A_N & 0 \end{bmatrix} \times \begin{bmatrix} \gamma_1 \\ . \\ . \\ . \\ \gamma_N \\ \lambda_0 \end{bmatrix} = \begin{bmatrix} 0 \\ . \\ . \\ . \\ 0 \\ \bar{L} \end{bmatrix} \quad (3)$$

Once the circulation is found, the optimal camber $(dz/dx = ZX_i)$ to support the minimum drag producing lift is determined from the following:

$$ZX_i = (a_{i,1}\gamma_1 + \cdots + a_{i,n}\gamma_n)A_i \quad (4)$$

Resulting optimal warp ZX_i is separated into spanwise twist and camber. The condition for max range and endurance for jet and prop planes can be applied to stop the process for incrementing the lift. The condition for max range of Jet- plane is $\left(\sqrt{C_L}/C_D\right)_{max}$ i.e. $C_{Di} = C_{D0}/3$. This condition for max endurance of Jet - plane is $(C_L/C_D)_{max}$ i.e. $C_{Di} = C_{D0}$ which is the also condition for max range for IC/Prop driven planes. The conditions for max endurance for IC/Prop is governed by $\left(C_L^{3/2}/C_D\right)_{max}$ i.e. $C_{Di} = 3C_{D0}$.

The constraint of pitching moment is considered in addition to lift constraint to generate reflex camber by introducing RCF. Objective function (F) for the drag minima, constrained lift and specified value of pitching moment is written in the Lagrange form using Lagrange multipliers (λ_0, λ_1) as given below by Eq. (5).

$$F = D + \lambda_0(LIF \times L - \bar{L}) + \lambda_1(M_y * RCF - \bar{M_y}) \quad (5)$$

The value of $\bar{M_y}$ is now specified, that is obtained by reducing the pitching moment which is obtained for the lift constraint alone. The matrix of optimization is given by Eq. (6) which is obtained by differentiating objective function (F) w.r.t circulation [5].

$$\begin{bmatrix} 2A_1a_{1,1} & . & . & . & . & (A_1a_{1,N}+A_Na_{N,1}) & A_1 & A_1XC_1 \\ . & & & & & . & . & . \\ . & & & & & . & . & . \\ . & & & & & . & . & . \\ (A_Na_{N,1}+A_1a_{1,N}) & . & . & . & . & 2A_Na_{N,N} & A_N & A_NXC_N \\ A_1 & . & . & . & . & A_N & 0 & 0 \\ A_1XC_1 & . & . & . & . & A_NXC_N & 0 & 0 \end{bmatrix} \times \begin{bmatrix} \gamma_1 \\ . \\ . \\ . \\ \gamma_N \\ \lambda_0 \\ \lambda_1 \end{bmatrix} = \begin{bmatrix} 0 \\ . \\ . \\ . \\ 0 \\ \bar{L} \\ \bar{M}_y \end{bmatrix} \quad (6)$$

where $XC_1, \ldots XC_N$ are distances of panel control points from y-axis and $a_{i,j}$ are influence coefficient towards downwash velocities. The solution of this matrix for given $\bar{L}$ & $\bar{M_y}$ values result in optimal circulation from where pressure difference coefficient, lift, drag, and pitching moment and bending moment are determined.

Morphing technology involves altering the aircraft' shape in response to external conditions. By adapting the shape and structural features of wings, morphing aircraft can achieve improved lift-to-drag ratios. Morphing is developed by freezing some slopes of camber that are not intended for variations.

Objective function (F) now for the drag minima is formed as below for the case where certain number of `m` panels are not allowed to undergo change in shape. The slopes of these panels are represented as $\overline{ZX}_{fix}$. In this equation $\overline{L}$ is the constrained value of lift, i.e. value of lift before optimization, and λ used as Lagrange multiplier [6-11]:

$$F = D + \lambda_0\left(L - \overline{L}\right) + \sum_{l=N-m+1}^{N} \lambda_l \left(ZX_l - \overline{ZX}_l\right)_{fix} \tag{7}$$

Matrix of optimization given by Eq. (8) is obtained by differentiation of the objective function (F) w.r.t circulation. The matrix provides the optimum circulation values γ_1 γ_N for the minimum induced drag, from where the lift and drag are calculated, and new camber line is determined.

$$\begin{bmatrix} 2A_1a_{1,1} & \cdots & A_1a_{1,N}+A_Na_{N,1} & A_1 & af_{N-m+1,1} & \cdots & af_{N,1} \\ \cdot & \cdots & \cdot & \cdot & \cdot & \cdots & \\ \cdot & \cdots & \cdot & \cdot & \cdot & \cdots & \\ \cdot & \cdots & \cdot & \cdot & \cdot & \cdots & \\ A_Na_{N,1}+A_1a_{1,N} & \cdots & 2A_Na_{N,N} & A_N & af_{N-m+1,N} & \cdots & af_{N,N} \\ A_1 & & A_N & 0 & & & \cdot \\ af_{N-m+1,1} & \cdots & af_{N-m+1,N} & \cdot & & & \cdot \\ \cdot & & \cdot & \cdot & & & \cdot \\ \cdot & & \cdot & \cdot & & & \cdot \\ af_{N,1} & \cdots & af_{N,N} & 0 & 0 & 0\ 0 & 0 \end{bmatrix} \times \begin{bmatrix} \gamma_1 \\ \gamma_2 \\ \cdot \\ \cdot \\ \gamma_N \\ \lambda_{N-m+1} \\ \lambda_{N-m+2} \\ \cdot \\ \cdot \\ \lambda_N \end{bmatrix} = \begin{bmatrix} 0 \\ \cdot \\ \cdot \\ \cdot \\ \cdot \\ \overline{L} \\ \left(\overline{ZX}_{N-m+1}\right)_{fix} \\ \cdot \\ \cdot \\ \left(\overline{ZX}_N\right)_{fix} \end{bmatrix} \tag{8}$$

Drag is determined from equation below:

$$D\begin{bmatrix} (a_{1,1}\gamma_1 + \ldots + a_{1,N}\gamma_N)\gamma_1 A_1 + (a_{2,1}\gamma_1 + \ldots + a_{2,N}\gamma_N)\gamma_2 A_2 \\ + \ldots\ldots\ldots\ldots\ldots\ldots + (a_{N,1}\gamma_1 + \ldots + a_{N,N}\gamma_N)\gamma_N A_N \end{bmatrix}_{min} \tag{9}$$

The optimal warp is given by Eqn. (4).

Aerodynamic optimization of wing in the presence of canard is developed through the objective function (F) for the drag (D) minima as below, where L is lift and $\overline{L}$ is constrained value of lift, λ_l are Lagrange multipliers, and $\overline{ZX^C}$ are constrained values of these canard slopes, i.e. the canard camber before and after the wing optimization, which are retained as invariants [12-14].

$$F = D + \lambda_0\left(L - \overline{L}\right) + \sum_{l=1}^{m} \lambda_l \left(ZX^C - \overline{ZX^C}\right)$$

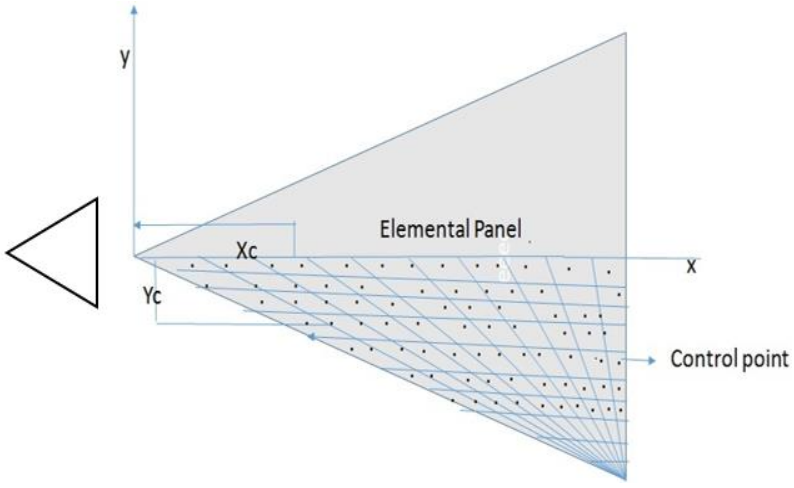

Figure 2. *Canard and wing arrangement.*

Figure 2 shows such an arrangement. Canard of any configuration can be positioned at various heights and distances from wing apex. Differentials of this function w.r.t circulation γ results in the matrix below. In the equation above, the fixed slopes ($\overline{ZX_1^C}$ $\overline{ZX_m^C}$) remain invariant and $\overline{L}$ does not vary. Matrix of optimisation is developed that is given by Eq. (10).

$$\begin{bmatrix} & & & & & & & & & & A_1^C & a_{1,1}^{CC} & . & . & a_{m,1}^{CC} \\ & & & & & & & & & & . & . & & & \\ & & [X1] & & & & & [X2] & & & . & . & & & \\ & & & & & & & & & & A_m^C & a_{1,m}^{CC} & . & . & a_{m,m}^{CC} \\ & & & & & & & & & & A_1^W & a_{1,1}^{WC} & . & . & a_{m,1}^{WC} \\ & & & & & & & & & & . & . & & & \\ & & [X3] & & & & & [X4] & & & . & . & & & \\ & & & & & & & & & & . & . & & & \\ & & & & & & & & & & A_n^W & a_{1,n}^{WC} & . & . & a_{m,n}^{WC} \\ A_1^C & . & . & . & A_m^C & A_1^W & . & . & . & A_n^W & 0 & 0 & . & . & 0 \\ a_{1,1}^{CC} & . & . & . & a_{m,1}^{CC} & a_{1,1}^{WC} & . & . & . & a_{1,n}^{WC} & 0 & 0 & . & . & 0 \\ . & & & & & & & & & . & . & . & & & \\ . & & & & & & & & & . & . & . & & & \\ . & & & & & & & & & . & . & . & & & \\ a_{m,1}^{CC} & & & & a_{m,m}^{CC} & a_{m,1}^{WC} & & & & a_{m,n}^{WC} & 0 & 0 & . & . & 0 \end{bmatrix} X \begin{bmatrix} \gamma_1^C \\ . \\ . \\ \gamma_m^C \\ \gamma_1^W \\ . \\ . \\ . \\ \gamma_n^W \\ \lambda_0 \\ \lambda_1 \\ . \\ . \\ . \\ \lambda_m \end{bmatrix} = \begin{bmatrix} 0 \\ . \\ . \\ . \\ . \\ . \\ . \\ . \\ 0 \\ \overline{L} \\ \overline{ZX_1^C} \\ . \\ . \\ . \\ \overline{ZX_m^C} \end{bmatrix} \quad (10)$$

Where

$$[X1] = \begin{bmatrix} 2A_1^C a_{1,1}^{CC} & . & . & (A_1^C a_{1,m}^{CC} + A_m^C a_{m,1}^{CC}) \\ . & & & \\ . & & & \\ (A_m^C a_{m,1}^{CC} + A_1^C a_{1,m}^{CC}) & & & 2A_m^C a_{m,m}^{CC} \end{bmatrix}$$

$$[X2] = \begin{bmatrix} (A_1^C a_{1,1}^{WC} + A_1^W a_{1,m}^{CW}) & . & . & (A_1^C a_{1,n}^{WC} + A_n^W a_{n,1}^{CW}) \\ . & & & \\ . & & & \\ (A_m^C a_{m,1}^{WC} + A_1^W a_{1,m}^{CW}) & & & (A_m^C a_{m,n}^{WC} + A_n^W a_{n,m}^{CW}) \end{bmatrix}$$

$$[X3] = \begin{bmatrix} (A_1^W a_{1,1}^{CW} + A_1^C a_{1,1}^{WC}) & . & . & (A_1^W a_{1,m}^{CW} + A_{nm}^C a_{m,1}^{WC}) \\ . & & & \\ . & & & \\ (A_n^W a_{n,1}^{CW} + A_1^C a_{1,n}^{WC}) & & & (A_n^W a_{n,m}^{CW} + A_m^C a_{m,n}^{WC}) \end{bmatrix}$$

$$[X4] = \begin{bmatrix} 2A_1^W a_{1,1}^{WW} & . & . & (A_1^W a_{1,n}^{WW} + A_n^W a_{1,n}^{WW}) \\ . & & & \\ . & & & \\ (A_n^W a_{n,1}^{WW} + A_1^W a_{1,n}^{WW}) & & & 2A_n^W a_{n,n}^{WW} \end{bmatrix}$$

Here γ are the optimum values of circulation that result in minimum drag keeping the lift same, \`A\` are panel areas, and \`$a_{i,j}$\` are influence coefficients. Suffix *m* indicates the number of panels on canard and *n* indicates number of panels on wing [12].

The matrix is solved for the optimal solution for γ values. Once the optimal circulation is determined the drag can be calculated from Eq. (11). Minimum drag is expressed from optimal circulation by equation below:

$$D_{min} = \rho U \textstyle\sum_{i=1}^{m} [\sum_{j=1}^{m} (a_{i,j}^{CC} \gamma_j^C) \gamma_i^C A_i^C]$$

$$+ \rho U \textstyle\sum_{i=1}^{m} [\sum_{j=1}^{n} (a_{i,j}^{WC} \gamma_j^W) \gamma_i^W A_i^W]$$

$$+ \rho U \textstyle\sum_{i=1}^{n} [\sum_{j=1}^{n} (a_{i,j}^{WW} \gamma_j^W) \gamma_i^W A_i^W]$$

$$+ \rho U \sum_{i=1}^{n}\left[\sum_{j=1}^{m}\left(a_{i,j}^{CW}\gamma_j^C\right)\gamma_i^C A_i^C\right] \tag{11}$$

Lift is given by Eq. (12).

$$L = \rho U[A_1^C\gamma_1^C + \cdots + A_m^C\gamma_m^C] + \rho U[A_1^W\gamma_1^W + \cdots + A_n^W\gamma_n^W] \tag{12}$$

Optimal panel warp at any panel is given by Eq. (13) & (14).

$$ZX_i^C = (a_{i,1}^{CC}\gamma_1^C + \cdots + a_{i,m}^{CC}\gamma_m^C)A_i^C + (a_{i,1}^{WC}\gamma_1^W + \cdots + a_{i,n}^{WC}\gamma_n^W)A_i^C \tag{13}$$

$$ZX_i^W = (a_{i,1}^{WW}\gamma_1^W + \cdots + a_{i,n}^{WW}\gamma_n^W)A_i^W + (a_{i,1}^{CW}\gamma_1^C + \cdots + a_{i,m}^{CW}\gamma_m^C)A_i^W \tag{14}$$

Superscript `c` refers to canard,`w` refers to wing, `cc` refers to canard on canard, `ww` refers to wing on wing, `wc ` refers to wing on canard and `cw` refers to canard on wing.

Transonic Flow: Computations of transonic flow are progressed to study the effect of drag rise in transonic regime. Transonic small perturbation equation below is used, where γ is the ratio of specific heats [15-17].

$$\left[\left(1-M^2\right)\phi_x\right]_x + \phi_{yy} + \phi_{zz} = 0 \tag{15}$$

where $1-M^2 = 1-M_\infty^2 - K\phi_x$ and $K = \frac{2}{U}\left[1+\frac{\gamma-1}{2}M_\infty^2\right]M_\infty^2$.

Equation is solved with finite difference methodology with line relaxation process. Mass conservative form is useful for accuracy of results, i.e., Eqn. (16) to refer. Suffix i, j, and k refer to index of panel in x, y, and z directions respectively.

$$p_{i,j,k} + q_{i,j,k} + r_{i,j,k} - (\mu_{i,j,k}\ p_{i,j,k} - \mu_{i-1,j}\ p_{i-1,i,k}) = 0 \tag{16}$$

μ provide the conservation in mass flax.
p, q and r are the central difference operators.

$\mu_{i-1,\,j,\,k} = 0,\ \mu_{i,\,j,\,k} = 0$ for elliptic region

$\mu_{i-1,\,j,\,k} = 1,\ \mu_{i,\,j,\,k} = 1$ for hyperbolic region

$\mu_{i-1,\,j,\,k} = 0,\ \mu_{i,\,j,\,k} = 1$ for sonic point operator

$\mu_{i-1,\,j,\,k} = 1,\ \mu_{i,\,j,\,k} = 0$ for shock point operator

The computational plane from the geometric plane is developed in the following manner:

$$\xi = \frac{x - x_{1e}}{x_{te} - x_{le}},\ \eta = y,\ \varsigma = z \tag{17}$$

Using this transformation, the values of ϕ derivatives can be written as below:

$$\phi_x = \phi_\xi\ \xi_x,\ \phi_y = \phi_\xi\ \xi_y + \phi_\eta,\ \phi_z = \phi_\zeta,$$

$$\varphi_{xx} = (\varphi_\xi\ \xi_x)_\xi\ \xi_x$$

$$\varphi_{yy} = (\varphi_\xi\ \xi_y + \varphi_\eta)_\xi\xi_y + (\varphi_\xi\ \xi_y + \varphi_\eta)_\eta$$

$$\phi_{zz} = \phi_{\xi\,\xi}$$

Using above equations, the transonic small perturbation equation is written as below:

$$\left(1-M^2\right)\left(\phi_\xi\ \xi_x\right)_\xi + \frac{\xi_y}{\xi_x}\left(\phi_\xi\ \xi_y + \phi_\eta\right)_\xi + \frac{1}{\xi_x}\left(\phi_\xi\ \xi_y + \phi_\eta\right)_\eta + \frac{1}{\xi_x}\phi_{\zeta\zeta} = 0 \tag{18}$$

with $\xi_x = 1/c$, and $\xi_y = \tan\wedge/c$.

or

$$\left[\left(1-M^2\right)\ \xi_x^2 + \xi_y^2\right]\ \varphi_{\xi\,\xi} + \xi_y\left(\varphi_{\eta\,\xi} + \varphi_{\xi\,\eta}\right) + \varphi_{\eta\,\eta} + \varphi_{\varsigma\,\varsigma} = 0 \tag{19}$$

Condition for elliptic region for equations (18) or (19) is $\left[(1 - M^2)\ \xi_x^2 + \xi_y^2\right] > 0$.

Condition of the hyperbolic region is

$$\left[(1 - M^2)\ \xi_x^2 + \xi_y^2\right] < 0$$

The derivatives of φ are determined from following equations.

$$(\phi_\eta)_\xi = \frac{\phi_{\eta_{i+1,j,k}} - \phi_{\eta_{i-1,j,k}}}{\xi_{i+1,j,k} - \xi_{i-1,jk}}$$

$$= \frac{\left(\varphi_{i+1,j+1,k} - \varphi_{i+1,j-1,k}\right)}{\left(\xi_{i+1,j,k} - \xi_{i-1,jk}\right)\left(\eta_{i+1,j+1,k} - \eta_{i+1,j-1,k}\right)}$$

$$- \frac{\left(\varphi_{i-1,j+1,k} - \varphi_{i-1,j-1,k}\right)}{\left(\xi_{i+1,j,k} - \xi_{i-1,j,k}\right)\left(\eta_{i-1,j+1,k} - \eta_{i-1,j-1,k}\right)} \quad (20)$$

$$(\varphi_\xi)_\eta = \frac{\varphi_{\xi_{i,j+1,k}} - \varphi_{\xi_{i,j-1,k}}}{\eta_{i,j+1,k} - \eta_{i,j-1,k}} = \frac{\left(\varphi_{i+1,j+1,k} - \varphi_{i-1,j+1,k}\right)}{\left(\eta_{i,j+1,k} - \eta_{i,j-1,k}\right)\left(\xi_{i+1,j+1,k} - \xi_{i-1,j+1,k}\right)}$$

$$- \frac{\left(\varphi_{i+1,j-1,k} - \varphi_{i-1,j-1,k}\right)}{\left(\eta_{i,j+1,k} - \eta_{i,j-1,k}\right)\left(\xi_{i+1,j-1,k} - \xi_{i-1,j-1,k}\right)} \quad (21)$$

$$(\varphi_\eta)_\xi = \frac{\varphi_{\eta_{i,j,k}} - \varphi_{\eta_{i-2,j,k}}}{\xi_{i,j,k} - \xi_{i-2,j,k}}$$

$$= \frac{\left(\varphi_{i,j+1,k} - \varphi_{i,j-1,k}\right)}{\left(\xi_{i,j,k} - \xi_{i-2,j,k}\right)\left(\eta_{i,j+1,k} - \eta_{i,j-1,k}\right)}$$

$$- \frac{\left(\varphi_{i-2,j+1,k} - \varphi_{i-2,j-1,k}\right)}{\left(\xi_{i,j,k} - \xi_{i-2,j,k}\right)\left(\eta_{i-2,j+1,k} - \eta_{i-2,j-1,k}\right)} \quad (22)$$

$$(\phi_\xi)_\eta = \frac{\phi_{\xi_{i,j+1,k}} - \phi_{\xi_{i,j-1,k}}}{\eta_{i,j+1,k} - \eta_{i,j-1,k}}$$

$$= \frac{\left(\varphi_{i,j+1,k} - \varphi_{i-2,j+1,k}\right)}{\left(\eta_{i,j+1,k} - \eta_{i,j-1,k}\right)\left(\xi_{i,j+1,k} - \xi_{i-2,j+1,k}\right)}$$

$$- \frac{\left(\varphi_{i,j-1,k} - \varphi_{i-2,j-1,k}\right)}{\left(\eta_{i,j+1,k} - \eta_{i,j-1,k}\right)\left(\xi_{i,j-1,k} - \xi_{i-2,j-1,k}\right)} \quad (23)$$

Equation (19) is transformed into difference equation through above equations and solved through line relaxation process. In the local supersonic region $\left[(1 - M^2)\ \xi_x^2 + \xi_y^2\right] < 0$ condition provides the up-wind conservation for appropriating the directional bias.

Grid Clustering: Grids need to be clustered around the shock wave. `W` a weighted length function is useful for such clustering [16, 17]. Consider the following weight function based on gradient of variable u, where β can be adjusted when solution gradient becomes high (which is representative of shock wave in our case).

$$W(x) = \frac{1}{\sqrt{1+\beta^2 u_x^2}},\ \beta = \sqrt{|1 - M^2|}$$

We need weight function $W(x)$ in terms of computational domain $W(\xi)$, as below

$$W(\xi) = \frac{1}{\sqrt{1+\frac{\beta^2}{x_\xi^2}u_\xi^2}}$$

Differentiating wight function w.r.t ξ

$$W_\xi = -\frac{\beta^2}{2}\left[\frac{\frac{2}{x_\xi^2}u_\xi u_{\xi\xi} - 2\frac{x_{\xi\xi}}{x_\xi^3}u_\xi^2}{\left(1+\frac{\beta^2}{x_\xi^2}u_\xi^2\right)^{3/2}}\right] = \frac{\beta^2 u_\xi\left(\frac{x_{\xi\xi}}{x_\xi}u_\xi - u_{\xi\xi}\right)}{x_\xi^2\left(1+\frac{\beta^2}{x_\xi^2}u_\xi^2\right)^{3/2}} \quad (24)$$

Thus,

$$\frac{W_\xi}{W} = \frac{\beta^2 u_\xi\left(\frac{x_{\xi\xi}}{x_\xi}u_\xi - u_{\xi\xi}\right)}{x_\xi^2+\beta^2 u_\xi^2} \quad (25)$$

for example, in our case of grid generation

$$u_{xx} = \frac{u_{\xi\xi}}{x_\xi^2} - \frac{u_\xi x_{\xi\xi}}{x_\xi^3} = \frac{u(\xi_{i+1})-2u(\xi_i)+u(\xi_{i-1})}{\left(\frac{x_{i+1}-x_{i-1}}{2}\right)^2} - \frac{\left(u(\xi_{i+1})-u(\xi_{i-1})\right)(x_{i+1}-2x_i+x_{i-1})}{2\left(\frac{x_{i+1}-x_{i-1}}{2}\right)^3} \quad (26)$$

If the grids are coarse, solutions are faster, however finer grids are needed which take larger time for convergence for accurate values. Multigrid techniques are helpful for faster convergence of solutions. Before the geometric multigrid scheme can be applied, the coarser grids must be generated.

Effect of Ground Proximity: The effect of solid boundary presence on wing is modeled by taking mirror image of equal and opposite strength of panels. The height of wing above ground is varied and its effect on aerodynamic coefficients is determined. Effects of flap engagement are also considered. Wing is placed at height `h` above a horizontal plane, and an equal but opposite vortex system of carbon wing placed at depth `h` below the ground plane. The vertical velocity component induced at any point on the ground plane by one of the wing vortices is made equal and opposite to that due to the carbon wing. This is done to make the net vertical velocity induced at any point on the solid boundary as zero [18, 19]. Figure 3 shows the schematics of wing above the ground and carbon wing below the ground at the same distance from ground.

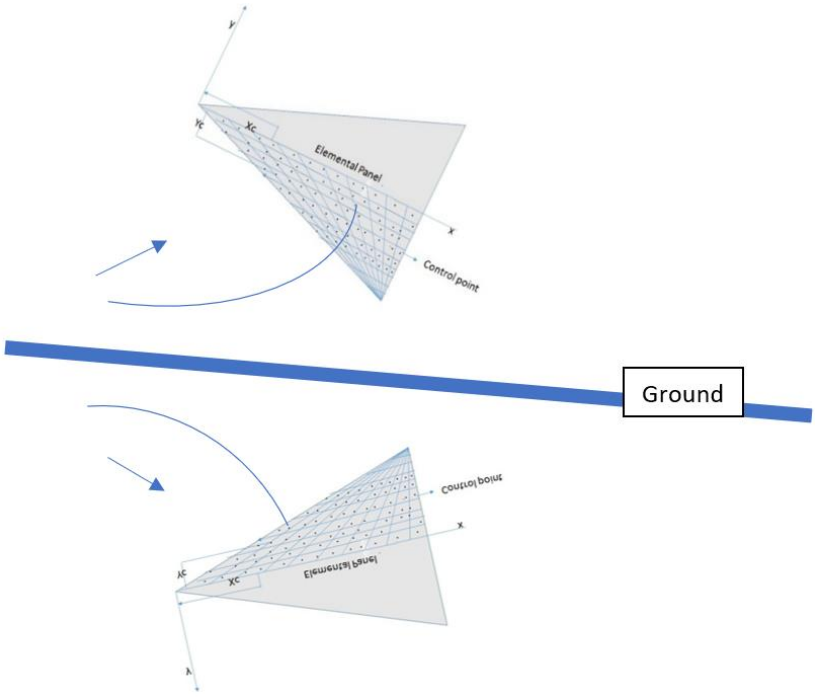

Figure 3. *Schematics of wing above the ground and carbon wing (inverted image) below the ground. Arrow indicates the flow direction.*

The circulation strength of panels of both wings is determined from matrix given by Eq. (27), Superscript herein are abbreviated as below:

W- Referred wing
C-Carbon wing
WOW-Influence of wing on wing
COW-Influence of carbon wing on wing
COC-Influence of carbon wing on carbon wing

WOC-Influence of wing on carbon wing

$$\begin{bmatrix} a_{i,j}^{WOW} & a_{i,j}^{COW} \\ a_{i,j}^{WOC} & a_{i,j}^{COC} \end{bmatrix} \begin{bmatrix} \gamma_i^W \\ \gamma_i^C \end{bmatrix} = \begin{bmatrix} w_i^W \\ -w_i^w \end{bmatrix} \tag{27}$$

The r.h.s. matrix of Eqn. (27) forms the boundary condition of tangential flow on the camber line. *It may be noted that* $[\gamma_i^w] = -[\gamma_i^c]$. The first matrix of this equation comprises of influence coefficients given by Eqns. (28) and second matrix comprises of unknown circulations that form the solution for circulation, from where the pressure difference coefficients are determined. Aerodynamic characteristics of the wing are analysed for varied ground proximities. As the wing operates closer to the ground, the lift is expected to increase due to higher pressure build up under the surface of wing. Changes in lift, induced drag and pitching moment coefficients are analysed.

$$a_{i,j}^{wow} = \begin{pmatrix} a_{1,1}^{wow} & \cdots & a_{1,n}^{wow} \\ \cdot & \cdot & \cdot \\ \cdot & \cdot & \cdot \\ \vdots & \ddots & \vdots \\ a_{n,1}^{wow} & \cdots & a_{n,n}^{wow} \end{pmatrix} \quad a_{i,j}^{cow} = \begin{pmatrix} a_{1,1}^{cow} & \cdots & a_{1,n}^{cow} \\ \cdot & \cdot & \cdot \\ \cdot & \cdot & \cdot \\ \vdots & \ddots & \vdots \\ a_{n,1}^{cow} & \cdots & a_{n,n}^{cow} \end{pmatrix}$$

$$a_{i,j}^{woc} = \begin{pmatrix} a_{1,1}^{woc} & \cdots & a_{1,n}^{woc} \\ \cdot & \cdot & \cdot \\ \cdot & \cdot & \cdot \\ \vdots & \ddots & \vdots \\ a_{n,1}^{woc} & \cdots & a_{n,n}^{woc} \end{pmatrix} \quad a_{i,j}^{coc} = \begin{pmatrix} a_{1,1}^{coc} & \cdots & a_{1,n}^{coc} \\ \cdot & \cdot & \cdot \\ \cdot & \cdot & \cdot \\ \vdots & \ddots & \vdots \\ a_{n,1}^{coc} & \cdots & a_{n,n}^{coc} \end{pmatrix} \tag{28}$$

A flare model for landing manoeuvre in form of exponential function can be considered for studies, pl see Eq. (29). This is the critical part of the landing when the pilot pulls back on the yoke, increasing the alpha to reduce the aircraft' vertical speed for a smooth touchdown. A flare manoeuvre is the action of gently raising an aircraft' nose just before touchdown to slow the rate of descent and set the appropriate landing attitude, resulting in a smoother landing. In control systems, the time constant (τ, or tau) is a measure of how quickly a first-order system responds to a step input, specifically the time it takes to reach approximately 63% of its final steady-state value. The parameter dominating the curvature of flare is this time constant. Generally, the flare time constant is determined based on the distance between the transmitter point and the touchdown point. The method involves in using an exponential function, its derivative, the glide slope angle, and the distance. A smaller time constant indicates a faster system response, while a larger time constant signifies a slower response. This parameter is considered to represent flare trajectory given by equation below. Wing loading and lift coefficient influence this parameter.

$$h_{flare} = h_0 e^{-t/\tau} \tag{29}$$

Here, h_o is the initial value of height of starting of flare manoeuvre and h_{flare} is height of flare manoeuvre at time `$t$`.

$\tau = -\frac{Usin\gamma}{g \times \Delta n_z}$, where `γ` is the approach angle before initiation of flare manoeuvre, which is the glide slope angle and is generally around 3^0 to 4^0.

The value of time constant of around three to four seconds is normally taken for modeling the flare manoeuvre, and Δn_z is the value of vertical acceleration at the initiation of flare manoeuvre. Time constant is directly proportional to lift coefficient and inversely proportional to wing loading. The latter of which has little choice because it is governed by the max all up weight and the fuel that is to be expanded. The lift coefficient during landing is approximately eight/nine times its value in flight. A lower lift coefficient is in favour of lesser time constant. Lower lift coefficient and higher drag coefficient are favouable for landing manoeuvre. Drag coefficient can be varied through leading edge flap deflection. A code is developed that gives information on % changes in lift, drag, and pitching moment as the height is varied to set a more appropriate time constant value.

3. Results and Discussions

Mach number is taken as 0.75, and value of C_{D0} is arbitrarily taken as 0.02. Wing of following dimension is considered as candidate.

Leading edge sweep =0.489 rad
Trailing edge sweep =0.262 rad
Taper ratio =0.367
Aspect ratio =7.0

Flat surface wing and a low value of angle-of-attack is taken to start the optimisation process. The lift is incremented by setting an increased value of lift coefficient by a factor referred to as lift increment factor. It is done to increase camber at given alpha. The value of LIF is limited to 1.4, otherwise the camber becomes larger, and benefit of wash out gets substantially reduced. The whole process involves in finding the desired range criteria at a suitable alpha and lift increment factor combinations. Table 1 shows the process. Values of alpha, LIF, lift coefficient, drag coefficients, range criteria, max camber in % of local chords, root wash out value for off-loading alpha and camber, change in pitching moment and wing root

bending moment are shown in this Table. Super script (*) shows the values after applying the process. Decrease in ratio of pitching moment before and after optimisation process shows increase in this pitching moment because of optimisation which is due to chordwise rearward shift in pressure difference loading.

Criteria for maximum range for induced drag coefficient to be 1/3rd of profile drag is applied. It is driven from $\left(\sqrt{C_L}/C_D\right)_{max}$ condition and is highlighted in this Table 1. A combination of 3^0 of alpha with LIF value of 1.1 results in this condition. Max camber is 2.2% occurring at 40% of local chord location which is of reasonable value for application on a high-speed aircraft. Optimisation results in drag reduction of (0.0162-0.0063)/0.0162, which is 61%. Optimal warp so generated is broken into twist and camber. Washout value at wing root is used to off-load alpha, as well as it is taken out from camber. Remaining twist is neglected. This alpha for offloading is around 1^0. Reduced alpha is in favourable of lesser wing-body interference effects. Similar results are seen published in literature [1, 2, 4].

Figure 4 shows the pressure difference coefficient on the optimal surface wing. Fore tip area has larger pressure difference as compared to root portion. This is because of non-elliptic nature of spanwise lift of the swept wing. This shows the pressure difference coefficient values for such a design process. The shape of curves undergoes a total change because of optimisation. Peak loading lies at around 55% of local chord at tip in contrast to it being at around 65% of local chord at root. This happens because of vortical flow towards tips. Table 2 shows the data generated for these design conditions i.e M_∞=0.75, alpha= 3^0. This table gives the details of aerodynamic coefficients The resulting camber is shown in Figure 5 which is at the mean aerodynamic chord. This camber is uniformly applied across the span, thereby making it planar.

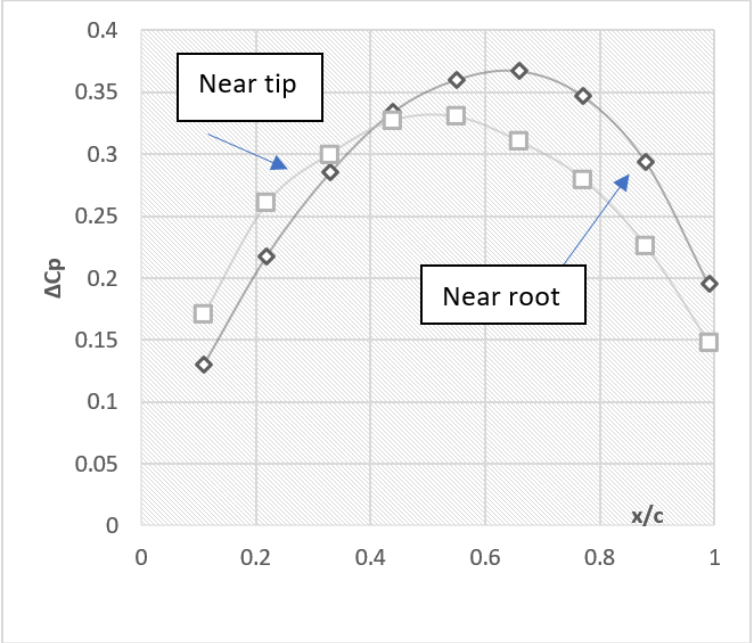

Figure 4. *Pressure différence coefficient, optimal surface.M_∞=0.75, alpha=3^0.*

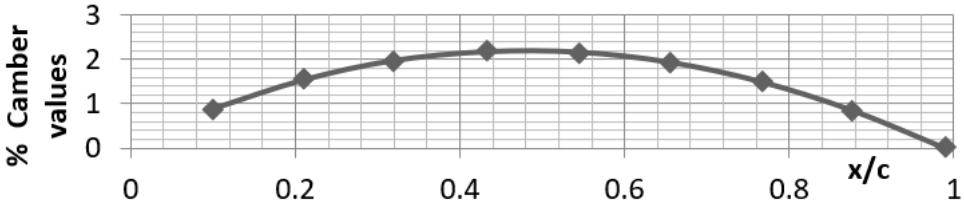

Figure 5. *Camber in% of chord at mean aerodynamic chord.*

Table 1. *Estimation of Camber for Maximum Range based upon Lift increment, M=0.75, C_{D0} =0.02. Range criteria* $\left(\sqrt{C_L}/C_D\right)_{max}$ *→C_{Di}=1/3C_{D0}.*

α⁰	Increment factor for C_L	C_L	C_{Di}		C_D=C_{D0}+C_{Di}		$\sqrt{C_L}/C_D$		(ζ/c) max camber in% of chord (bracket shows location in% of chord)	Root wash-out Values for off-loading Alpha	C_L/C_{Di}		My/My^*	Mx/Mx^*
	LIF		Before	After	Before	After	Before	After			Before	After		
	NIL	0.1872	0.0065	0.0023	0.0265	0.0223	16.32	19.40	1.36(40%)	0.0145rad (0.83deg)	28.8	81.39	0.849	1.027
2	1.2	0.2246	0.0078	0.0033	0.0278	0.0233	17.05	20.34	1.63(40%)	0.0104rad (0.59deg)	28.8	68.06	0.707	0.856
	1.4	0.2620	0.0091	0.0046	0.0291	0.0246	17.59	20.80	1.85(40%)	0.0063rad (0.36deg)	28.75	56.95	0.606	0.734
	NIL	0.281	0.0147	0.0052	0.0347	0.0252	15.27	21.03	2.0(40%)	0.0217rad (1.24deg)	19.11	54.04	0.849	1.028
3	1.1	0.309	0.0162	0.0063	0.0362	0.0263	15.35	21.13	2.2(40%)	0.0187rad (1.07deg)	19.07	49.05	0.772	0.934
	1.2	0.337	0.0176	0.0075	0.0376	0.0275	15.44	21.11	2.37(40%)	0.0156rad (0.89deg)	19.14	45.00	0.707	0.856

Thereafter, morphing is applied to this profile for the condition that C_{Di}=C_{D0} which results from the criteria of $(C_L/C_D)max$. It is applied to a limited region which is 20% of local chord from leading edge and 20% of local chord from trailing edge. These can also be visualised as the areas where flaps are generally formed. Mach number is taken as 0.5. Figure 6 shows results of morphed slopes. Straight line in this figure represents pre-morphed slopes and shows 60% mid region remaining invariant to changes in slopes. Similar results are seen reported in references 9, 10 and 11.

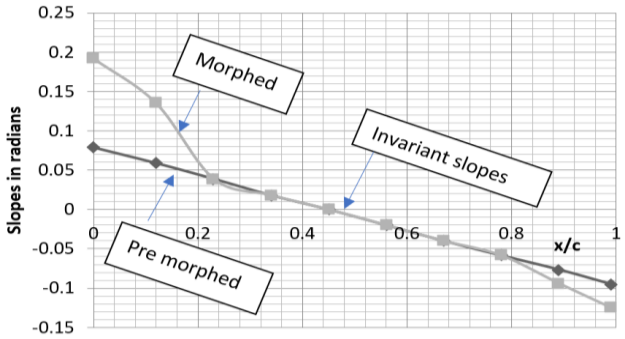

Figure 6. *Resulting camber slopes of pre-morphed and morphed Profiles, Mach number is taken as 0.5, alpha=3⁰.*

Transonic flow programme is applied to the wing camber designed for jet airplane range condition. Optimal camber of wing is superimposed with thickness of NACA 0009 airfoil. Developed wing template is shown in Figure 7. Transonic flow code is applied to this wing for $M_\infty = 0.9$, and alpha of 4^0. The flow field values of pressure coefficient are shown varying with z/c on upper surface. The strength of shock wave weakens as the z distance increases. Transonic code is further applied to a delta wing and to another a delta wing with integrated LEX (leading edge extension). LEX span is 1/3rd of wing span and LEX chord is half of wing root chord. Wing tips are slightly clipped to prevent infinite solutions towards tips. All data is generated for alpha equal to 4^0. Mach number is varied from subcritical to supercritical conditions. Figure 9 shows comparison of drag coefficients of these wings with Mach number variation. There is remarkably low transonic drag rise in case of LEX-Wing. Wing has the following Data.

Leading edge sweep=45^0
Trailing edge sweep=0^0
Aspect ratio=3.2
Taper ratio=0.1

Matrix involved in these techniques are highly diagonally concentred and has non-zero elements only on main diagonal and the two diagonals immediately above and below it. This poses the problem in parallelism support. Recent advances in parallel algorithms have addressed the computational demand of solving tridiagonal and block-tridiagonal systems on mod-

ern hardware. Artificial intelligence-based algorithms are increasingly used to analyze and classify the sparse matrices generated in Computational Fluid Dynamics (CFD) to optimize parallelization. These algorithms aim to identify structural properties (sparsity pattern, symmetry, diagonal dominance) to select the best partitioning strategy (e.g., domain decomposition) and solver.

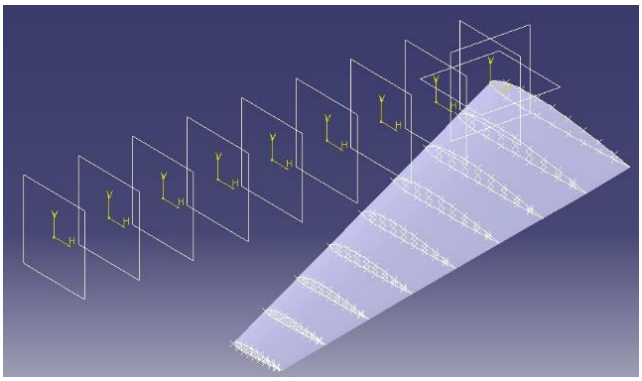

Figure 7. *Template of wing developed for max range condition of Jet aircraft.*

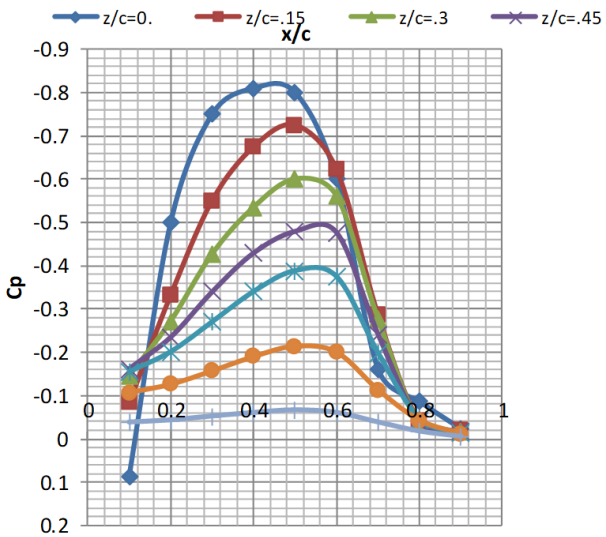

Figure 8. *Progressively varying field values of pressure coefficient on upper surface near root, $M_\infty = 0.9$, and Alpha= 4^0.*

Aerodynamic interference with ground is now studied. Wing of template at Figure 7 is considered. Aerodynamic coefficients with deployed flaps are worked out for working out flare manoeuvre. Following conditions are taken for this study:

Leading edge flap is taken full span and is 20% of local chord

Trailing edge flap is taken 60% of semi-span from root and is 30% of local chord

Mach number is taken as 0.25

Trailing edge flap deflection, δ_{tef}=25^0

Leading edge flap deflections δ_{lef} and alpha are varied to study the effect of aerodynamic characteristics of such combinations. It helps in selecting the value of leading edge flap deflection for flare manoeuvre. Table 3 shows such a data which is plotted in Figure 10. It can be seen from this figure that as the lift coefficient is increased at a constant value of induced drag coefficient, leading flap defection requirement gets increased. If lift coefficient is held at a constant value, induced drag coefficient gets reduced with increasing leading edge flap deflection. It shows the significant role of leading edge flap in reducing the induced drag coefficient. Table 4 shows the choice of aerodynamic coefficients for landing flare manoeuvre.

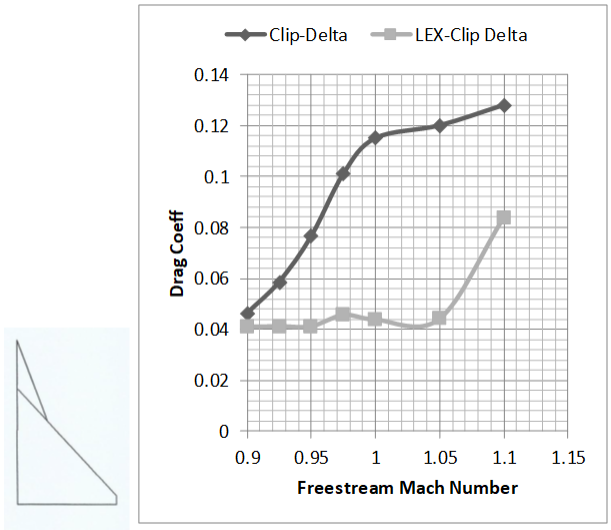

Figure 9. *Comparison of Drag Coefficients.*

With the deflected leading edge flaps, C_{Di}/C_L is higher for δ_{lef}=10^0, as compared to δ_{lef}=15^0, and therefore, this condition is taken for landing.

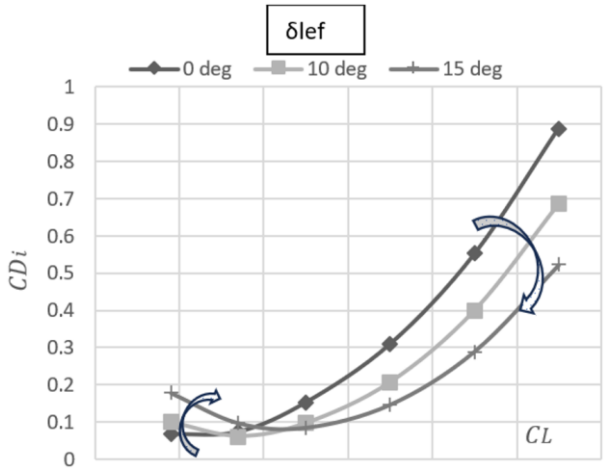

Figure 10. *The plot of lift coefficient vrs induced drag coefficient for varied leading edge flap deflections, M_∞=0.25 and δ_{tef}=25^0.*

Table 2. Design point Data.

M_∞=0.75, α=3⁰, LIF=1.1								
C_L	C_{Di}		C_{my}		My/My^*	C_{mx}		Mx/Mx^*
	Before	After	Before	After		Before	After	
0.309	0.0162	0.0063	0.2283	0.2957	0.772	0.2988	0.3198	0.934

Table 3. Aerodynamic coefficients with flaps deployment.

M_∞=0.25, and δ_{tef}=25⁰						
	δ_{lef}=0⁰		δ_{lef}=10⁰		δ_{lef}=15⁰	
Alpha	C_L	C_{Di}	C_L	C_{Di}	C_L	C_{Di}
-10⁰	0.462	0.067	0.416	0.099	0.362	0.177
-5⁰	0.873	0.074	0.829	0.062	0.780	0.096
0⁰	1.301	0.153	1.259	0.097	1.212	0.084
5⁰	1.754	0.310	1.712	0.207	1.669	0.146
10⁰	2.245	0.552	2.204	0.400	2.161	0.289
15⁰	2.789	0.89	2.748	0.687	2.705	0.522

Table 4. Choice of Aerodynamic coefficients with flaps deployment.

M_∞=0.25, and δ_{tef}=25⁰									
	δ_{lef}=0⁰			δ_{lef}=10⁰			δ_{lef}=15⁰		
Alpha	C_L	C_{Di}	C_{Di}/C_L	C_L	C_{Di}	C_{Di}/C_L	C_L	C_{Di}	C_{Di}/C_L
15⁰	2.789	0.89	0.319	2.748	0.687	0.25	2.705	0.522	0.19

Table 5. Lift coefficient and drag coefficient variation with decrease in height Mach No. 0.25 and Alpha =15⁰.

h/b	C_L	% change in C_L	C_{Di}
1.0	2.748	-	0.688
0.5	2.798	1.8%	0.697
0.25	2.930	4.7%	0.723
0.125	3.217	9.7%	0.790
0.0625	3.799	18.0%	0.947

Table 6. Effect of height variations on pitching moment coefficients with decrease in height, Mach No. 0.25 and Alpha =15^0.

h/b	C_{my}	ΔC_{my}	$\partial C_{my}/\partial h$
1.0	-2.298	-	
0.5	-2.338	-0.040	0.002
0.25	-2.443	-0.105	0.009
0.125	-2.671	-0.228	0.041
0.0625	-3.146	-0.475	0.173

The height is varied and aerodynamic coefficients computed; Table 5 is to refer. Figure 11 shows the% increase in Lift coefficient with decrease in height. This Table shows rising lift coefficient associated with deceasing height. This has an implication on floating tendency of plane while being close to runway and therefore is of significance in framing time constant as a variable with height for designing automatic landing.

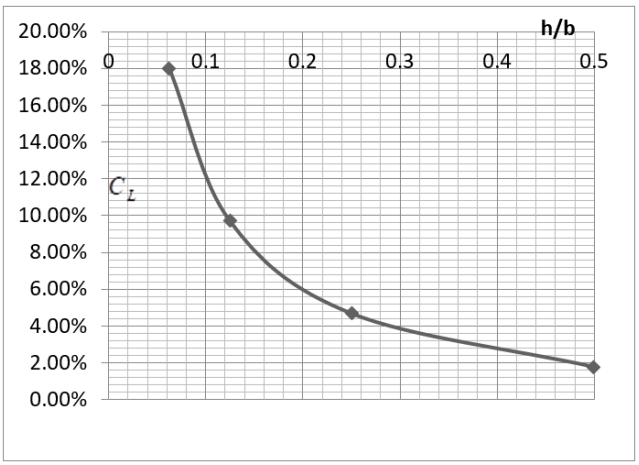

Figure 11. The% increase in lift coefficient during at landing.

Table 6 shows variation of pitching moment coefficient about leading edge (C_{my}), and its derivative with height. The growing negative pitching moment, as the height is lowered, indicates increasing strong nose down tendency being developed, thereby effecting pilots' control. Derivative of pitching moment with height is positive which indicates development of instability as a function of height variation. Figure 12 shows Pressure plots at two different spanwise stations under two extreme height conditions that are considered. There is larger increase in the value of ΔCp near root as compared to that towards the tip. Peak pressure occurs at around 75% of local cord in case of root station, whereas it is at around 65% of local chord in case of tip station; and that is shown by a dotted line in this figure. Adverse pressure gradients are stronger at root station compared to mild such gradients at tip station. The curves in these plots show unique follow-up.

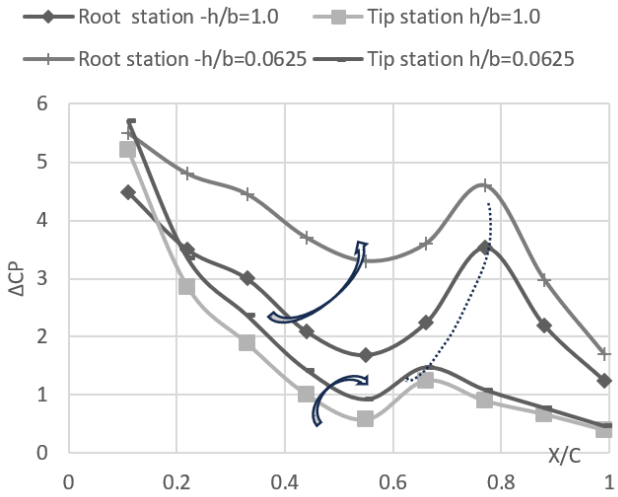

Figure 12. Pressure plots at two different spanwise stations under two extreme heights conditions considered during landing.

4. Conclusions

Aerodynamic optimisation applied herein has shown a large reduction in induced drag coefficient. A technique has been brought out to break optimal warp into twist and camber and lower the angle-of attack and camber by the washout value at root of optimised wing. The remaining camber is uniformly applied across the span and no twist is considered, thereby a planar wing is formed. A technique of morphing has been successfully developed and applied. Transonic flow field analysis has been developed and applied. The implication of deployment of leading-edge flap for flare maoneuvre is highlighted. The effect of ground proximity is analysed. There is nose down tendency that gets developed due to increases in pitching moment because of increase in lift coefficient, thereby requiring modelling of time constant as a function of lift coefficient.

Abbreviations

A	Panel Area
$a_{i,j}$	Influence Coefficient of j_{th} Panel on i_{th} Control Point
af	Influence Coefficient of Panels with Fixed Slopes
b	Span
c	Local Chord
ΔCp	Pressure Difference Coefficient
C_{D0}	Profile Drag Coefficient
C_{Di}	Induced Drag Coefficient
C_L	Lift Coefficient
C_{mx}	Wing Root Bending Moment Coefficient
C_{my}	Pitching Moment Coefficient About Wing Apex
D	Induced Drag
L	Lift
M_∞	Freestream Mach Number
M	Local Mach Number
M_x	Wing Root Bending Moment About Longitudinal Axis
M_y	Pitching Moment About y Axis
N	Number of Panels
U	Freestream Velocity
w	Downwash
x,y,z	Chordwise, Spanwise and Vertical Coordinates Respectively
ρ	Density
g	Gravitational Constant
α	Angle-of-Attack (Alpha)
φ	Velocity Potential Function
γ	Circulation Strength of Panels
δ_{lef}	Leading Edge Flap Deflection
δ_{tef}	Trailing Edge Flap Deflection
i	Control Point of Panel for Collocation of Downwash
j	Panel Index
le	Leading Edge
te	Trailing Edge

Author Contributions

Satish Chander Gupta: Methodology, Formal Analysis

Conflicts of Interest

The author declares no conflicts of interest.

References

[1] Lyu, Z. J.; Martins, J. R. R. A. "Aerodynamic Design Optimization Studies of a Blended-Wing-Body Aircraft", J. Aircraft. 2014, *51*, 1604–1617.

[2] Gupta, S. C., "Computational Algorithms for the Configuration Design," ICAS Paper No. 98-6.4.5, 21st International Council for the Aeronautical Sciences, September 13-18, 1998, Melbourne, Australia.

[3] Gupta, S. C., "Applied Computational Fluid Dynamics", Wiley India Pvt. Ltd. 2019.

[4] A. M. Morris, C. B. Allen, T. C. S. Rendall, "CFD based Optimization of airfoils Using Radial Basis Functions for Domain Element Parameterization and Mesh Determination", Int. J. Numerical Methods Fluids 58(March 2008) 822-860.

[5] Gupta, S. C., "OPSGER: Computer Code for Multi-Constraint Wing Optimisation", Journal of Aircraft, Vol. 25., No. 6, June 1988.

[6] Alexandar S. Goodman, "Conceptual Aerodynamic Design of Delta-type Tailless Unmanned Aircraft", International journal of Unmanned Systems Engineering, Vol. 2. No. S2, 2014.

[7] Null, W., and Shkarayev, S., "Effect of Camber on the Aerodynamics of Adaptive-Wing Micro Air Vehicle", Journal of Aircraft, Vol. 42, No. 6, 2005.

[8] B. K. S. Wood, and J. H. S. Fincham, "Aerodynamic Modelling of the Fish Bone Active Morphing Concept", Proceeding of RAeS, Applied Aerodynamic Conference, Bristol, UK, June 2014.

[9] J. H. S. Fincham & M. I. Friswell,` `Aerodynamic Optimisation of a Camber Morphing Aerofoil", Aerospace Science and Technology, Vol. 3, June 2015.

[10] Ahn, J., & Lee, D., "A Computational Study on the Aerodynamic Characteristics of a Flying-Wing MAV design", 30th AIAA Applied Aerodynamics Conference (2012).

[11] Gupta, S. C., "GENMAP: Computer Code for Mission Adaptive Profile Generation, "Journal of Aircraft, Vol. 25. No. 8, August 1988.

[12] Gupta, S. C., "COPTIM: Computer Code for Canard Coupled Wing Optimization", Canadian Aeronautics and Space Journal, Vol. 37, No. 4, December 1991.

[13] S. C. Gupta, "A Reconstructive Approach for Design of 3-D Low Drag Planar Wings", Journal of Aerospace Sciences and Technologies: Vol. 72, No. 1, Feb. 2020.

[14] Hummel, D. & Oelker, H. Chr. (1989). Effects of Canard position on the Aerodynamic Characteristics of a Close Coupled Canard Configuration at Low Speed. AGARD-CP-465.

[15] H. L. Atkins and H. A. Hassan, "Transonic Flow Calculations Using Euler Equations", AIA Journal, Vol. 21, No. 6, June 1983.

[16] Gupta, S. C., "TWING: Computer Code for Transonic Flow Analysis Over Wings", Presented at the 44 AGM of the Ae. S. I. at I. I. Sc., 11 December 1992, Bangalore.

[17] Gupta, S. C., "Transonic Flow Computations Past Optimally Warped Wings," ICTACEM – 98, Dec 1-5, 1998, IIT Kharagpur, India.

[18] Mongkol Thianwiboon, "Numerical Aerodynamics Analysis of a Reflexed Aerofoil, N60R, in Ground Effect with Regression Models", International Journal of Thermofluid Science and Technology, Vol. 9, Issue 1, Paper no. 090105, 2022.

[19] Mongkol Thianwiboon, "A Numerical Comparative Study of the Selected Cambered and Reflexed Aerofoils in Ground Effect", Engineering Journal, Volume 27, Issue 11, 2023.